# Dalton Transactions

Accepted Manuscript






ROYAL SOCIETY OF CHEMISTRY

www.rsc.org/dalton

# Magnetic Mesoporous Silica Nanoparticles for Potential Delivery of Chemotherapeutic Drugs and Hyperthermia

Cuilian Tao[a], Yufang Zhu[b]*

[a] School of Medical Instrument and Food Engineering, University of Shanghai for Science and Technology, 516 Jungong Road, Shanghai, 200093, China.

[b] School of Materials Science and Engineering, University of Shanghai for Science and Technology, 516 Jungong Road, Shanghai, 200093, China. Tel: +86-21-55271663;

Corresponding author:

Prof. Yufang Zhu

Tel: +86-21-55271663

Email: zjf2412@163.com

**Abstract:** Magnetic mesoporous silica (MMS) nanoparticles with controllable magnetization have been synthesized by encapsulating $Fe_3O_4$ nanoparticles in mesoporous silica matrix. The structure, magnetic heating capacity and dug delivery ability of MMS nanoparticles were evaluated. The results showed that MMS nanoparticles had the average particles size of 150 nm, and showed low cytotoxicity and efficient cell uptake ability. MMS nanoparticles exhibited a sustained drug release in the medium of pH 5.0, but a very slow release in the medium of pH 7.4. On the other hand, MMS nanoparticles could controllably generate heat to reach the hyperthermia temperature within a short time upon exposure to an alternating magnetic field due to the superparamagnetic behavior and controllable magnetization. Therefore, MMS nanoparticles could provide a promising multifunctional platform for the combination of chemotherapy and hyperthermia for cancer therapy.

**Keywords:** Magnetic nanoparticles, Mesoporous silica, Drug delivery, Hyperthermia

## 1. Introduction

Cancer is a disease caused by both a genetic predisposition and environmental factors, which has high mortality rate in worldwide. Chemotherapy is a common therapeutic approach relying on the use of toxic chemotherapeutic drugs, but recurrence often occurs due to the multidrug-resistance of tumor cells in chemotherapy [1].

To date, much effort has been made to develop efficient approaches that can enhance the therapeutic efficacy in cancer therapy [2-6]. Hyperthermia is a therapeutic technique based on deactivation of cancer cells by raising the temperature in the range of 43 $^{o}$C and 48 $^{o}$C [2-3]. At this temperature range, heat also increases the efficacy of different chemotherapeutic drugs [7]. Therefore, the combination of conventional chemotherapy with hyperthermia provides a promising strategy, which can produce synergistic therapeutic effects on tumor cells and reduce the required effective doses of anticancer drugs [8-11]. However, the key issue is that both conventional chemotherapy and hyperthermia should have the ability to deliver anticancer drugs and heat to the tumors simultaneously.

Studies demonstrated the possibility for the combination of chemotherapy and hyperthermia by the nanoparticle-based delivery systems [12]. In particular, magnetic nanoparticles (MNPs) offer a great potential as they can be loaded with anticancer drugs and heated under an external alternating magnetic field after localization in tumors [8-11]. At present, preparation of the MNPs-based delivery system is the most popular strategy for chemotherapy and hyperthermia [13]. One hand, the surface of MNPs was functionalized with an organic shell (cyclodextrin, dextran, DNA, etc.) in a way that the chemotherapeutic drugs are embedded with the shell [14-15]. On the other hand, the chemotherapeutic drugs

were loaded in thermo-responsive polymers and liposomes with embedded MNPs [16-19]. However, intravenous administration of organic lipoplexes or polyplexes often result in particle instability and nonspecific interaction with blood components that induce the side effects of opsonization, aggregation of red blood cells and platelet activation [20].

Therefore, more and more studies focused on the design and preparation of inorganic coatings or matrix for MNPs to form inorganic magnetic composite nanoparticles [21-24], such as silica, gold, hydroxyapatite, and graphene, which can not only deliver drugs through the adsorption of drugs on the surface of the nanoparticles, but also make the nanoparticles stable and biocompatible, and thereby be useful for hyperthermia. However, these cases often afford a low therapeutic dose for drug delivery due to the limited surface area.

Mesoporous silica nanoparticles (MSNs) have gained more and more attention catalysis, adsorption/separation, drug/gene delivery applications [25-29]. To date, MSNs have been considered as a promising candidate carrier for drug/gene delivery due to their high surface area, large pore volume and ease of surface functionalization [28-29]. Furthermore, encapsulation of MNPs in mesoporous silica matrix enhances the chemical stability of MNPs and avoids the potential toxicity effect of MNPs on cells [30]. Thus, it is a good choice to use magnetic mesoporous silica (MMS) nanoparticles as a platform for chemotherapy and hyperthermia.

To date, many studies have demonstrated the preparation of MMS nanoparticles for drug delivery or hyperthermia therapy [25, 31-44]. For example, Shi and coworkers reported the preparation of core/shell structured $Fe_3O_4/SiO_2$ mesoporous nanoparticles for sustained

drug release [31-32]. Qiao and coworkers synthesized monodisperse yolk-shell magnetic nanoparticles with a hierarchical porous structure, and these magnetic nanoparticles enhanced drug loading capacity and exhibited drug release behavior [33]. Sanchez and coworkers reported the fabrication of mesoporous maghemite-organosilica microspheres by spray-drying process, and for the first time proposed magnetic mesoporous microspheres as multifunctional platforms for MR imaging and hyperthermia therapy [34]. Sousa and coworkers prepared $Fe_3O_4$/SBA-15 mesoporous nanocomposite by impregnation of an iron precursor into SBA-15 framework, and hyperthermia tests indicated that the $Fe_3O_4$/SBA-15 nanocomposite had potential for localized hyperthermia treatment of cancers [35]. However, there are limited reports on describing MMS nanoparticles for the combination of chemotherapy and hyperthermia until now. Vallet-Regí and coworkers reported aerosol-assisted synthesis of magnetic microspheres composed of γ-$Fe_2O_3$ nanoparticles embedded in mesoporous silica matrix, and these magnetic microspheres showed the abilities to load and release therapeutic drugs and to conduct magnetic hyperthermia upon exposure to a low-frequency alternating magnetic field [36-37]. However, these magnetic microspheres were heterogeneous in particle size, ranging from 0.3 to 3 μm in diameter, which would be accumulated in organs due to the large particle size. Lu et al. synthesized magnetic iron oxide-loaded hollow mesoporous silica nanocapsules using polymer nanospheres as sacrificial templates, and found that these magnetic nanocapsules with particle size of 100 nm showed magnetic field induced heating and remotely triggered drug release capabilities, and thereby provide a platform for the combination of hyperthermia and chemotherapy [38].

In this study, we report a MMS nanoparticle-based drug delivery system for potential chemotherapy and hyperthermia. Preparation of monodisperse MMS nanoparticles with controllable magnetization involves the synthesis of superparamagnetic $Fe_3O_4$ nanoparticles by co-precipitation method and subsequently encapsulating $Fe_3O_4$ nanoparticles in mesoporous silica matrix by using sol-gel technique and hexadecyltrimethylammonium p-toluenesulfonate (CTAT) as structure-directing agent. The structure, magnetic heating capacity and drug delivery ability of MMS nanoparticles were investigated in detail.

## 2. Experimental

### 2.1 Chemicals

Tetraethyl orthosilicate (TEOS), triethanolamine (TEA), ethanol, hydrochloride acid (HCl, 36-38%), Ppotassium dihydrogen phosphate ($KH_2PO_4$), sodium hydroxide (NaOH), ferric chloride ($FeCl_3{\cdot}6H_2O$), ferrous chloride ($FeCl_2{\cdot}4H_2O$) were obtained from Sinopharm Chemical Reagent Co., Ltd. Doxorubicin hydrochloride (DOX) was obtained from Sangon Biotech (Shanghai) Co., Ltd. Hexadecyltrimethylammonium p-toluenesulfonate (CTAT) was obtained from Sigma-Aldrich. Ultrapure water was obtained from Millipore pure water system. All chemicals are analytical-reagent grade and used without further purification.

### 2.2 Synthesis of $Fe_3O_4$ nanoparticles

Magnetic $Fe_3O_4$ nanoparticles were synthesized according to the reported co-precipitation method with some modification [45]. Typically, 19.2 mmol $FeCl_3{\cdot}6H_2O$ and 19.2 mmol $FeCl_2{\cdot}4H_2O$ were dissolved in 25 ml of water under ultrasonication for 30 min, followed by the addition of 0.85 ml of HCl (36-38%). Then, 250 ml of NaOH aqueous

solution (1.5 mol/l) was added drop by drop to the obtained homogeneous yellow solution with continuously stirred and after that the mixture was kept vigorously stirring at 700 rpm at room temperature for 1 h. The black precipitates were collected with the help of a magnet and washed several times with ultrapure water and ethanol, and then dried in vacuum at 60 $^{o}$C for 24 h.

2.3 Synthesis of magnetic mesoporous silica (MMS) nanoparticles

Monodisperse MMS nanoparticles with uniform particle size were synthesized by using a sol-gel technique. Typically, 0.2 g, 0.3 g and 0.4 g of $Fe_3O_4$ nanoparticles were firstly dispersed in 36 ml of water under ultrasonication for 30min, respectively. Subsequently, 0.6836 g of CTAT and 4 g of TEA were added to each $Fe_3O_4$ suspension at 353 K with vigorously stirring for 1 h. Then, 5.58 ml of TEOS was rapidly added to each mixture, and the reaction was continued for another 2 h to form a blown colloidal suspension. The obtained blown colloidal nanoparticles were separated with a magnet, washed with ethanol for several times, and dried in vacuum at 60 $^{o}$C for 24 h. Finally, the dried colloidal nanoparticles were calcined at 540 $^{o}$C for 7 h to remove the surfactant CTAT and obtained MMS nanoparticles. Samples were named as $Fe_3O_4/mSiO_2$-1, $Fe_3O_4/mSiO_2$-2 and $Fe_3O_4/mSiO_2$-3, respectively.

2.4 Characterization

Transmission electron microscopy (TEM) images were obtained using a JEM-2100F transmission electron microscope at an acceleration voltage of 200 kV. The wide angle X-ray diffraction (WAXRD) patterns were obtained on a D8 ADVANCE powder diffractometer using Cu Kα1 radiation (1.5405 Å). UV–Vis absorption spectra were measured on a NanoDrop

2000C spectrophotometer. $N_2$ adsorption-desorption isotherms were obtained on a Micromeritics Tristar 3020 automated surface area and pore size analyzer at 77 K under continuous adsorption conditions. Brunauer-Emmett-Teller (BET) and Barrett-Joyner-Halenda (BJH) methods were used to determine the surface area and pore size distribution. Magnetization curves were carried out using a TF-WI-ZDYP V 3.0.4 vibrating sample magnetometer (VSM) at 298 K. Magnetic heating curves and specific absorption rate (SAR) of MMS nanoparticles were obtained on a DM100 magnetic hyperthermia analyzer (NanoScale Biomagnetics, Spain) at the magnetic field of 90-180 Gauss and the frequency of 409 kHz or 238 kHz.

2.5 Drug loading and release.

In this study, doxorubicin hydrochloride (DOX), an anticancer drug, was used as a model drug to evaluate the drug delivery ability of MMS nanoparticles. To load DOX into MMS nanoparticles, 30 mg of $Fe_3O_4/mSiO_2$-1, $Fe_3O_4/mSiO_2$-2 and $Fe_3O_4/mSiO_2$-3 nanoparticles were mixed with 6 ml of DOX solution in PBS (0.25 mg/ml), respectively. After 24 h of agitation under dark conditions, the DOX-loaded MMS nanoparticles were collected by centrifugation, and washed with PBS twice to remove DOX adsorbed on the surface of MMS nanoparticles. To estimate the DOX loading capacity, the supernatant and washed solutions were collected and the residual DOX content was estimated by measuring the absorbance values at 481 nm using UV-Vis analysis. Before determination, a calibration curve was recorded by NanoDrop 2000C Spectrophotometer.

To investigate the DOX release behavior from MMS nanoparticles, 30 mg of DOX-loaded $Fe_3O_4/mSiO_2$-1 (or DOX-loaded $Fe_3O_4/mSiO_2$-2 or DOX-loaded $Fe_3O_4/mSiO_2$-3)

nanoparticles was suspended by shaking in 10 ml of the release medium with pH 5.0 and pH 7.4 at 37 $^{o}$C. At predetermined time intervals, the release system was centrifuged and an aliquot (20 µl) of supernatant solution was taken out for UV-Vis analysis, and replaced with the same amount of fresh medium.

2.6 Magnetic heating capacity

Magnetic heating capacities of $Fe_3O_4$ and MMS ($Fe_3O_4$/m$SiO_2$-1, $Fe_3O_4$/m$SiO_2$-2 and $Fe_3O_4$/m$SiO_2$-3) nanoparticles were evaluated using a DM100 System (NanoScale Biomagnetics, Spain) and the temperature was measured with an optical fiber temperature sensors. $Fe_3O_4$ or MMS nanoparticles were dispersed in water to a concentration of 50 mg/ml. The suspension was heated under an alternating magnetic field of 90-180 Gauss in strength at 409 kHz and 238 KHz frequency for 20 min, respectively. The upper limited temperature was set up to be 80 $^{o}$C. The capacity of a magnetic material to absorb energy from an alternating magnetic field is quantified by the specific absorption rate (SAR).

2.7 Cell culture

Hela cell lines were maintained in MEM medium containing 10% fetal bovine serum, 100 units/mL penicillin, and 100 mg/mL streptomycin. Cells were cultured with the complete medium in 5% $CO_2$ at 37$^{o}$C. For all experiments, cells were harvested from sub-confluent cultures by the use of trypsin and were resuspended in fresh complete medium before plating.

2.8 In vitro cytotoxicity assay

An in vitro cytotoxicity assay for MMS nanoparticles was using a Cell Counting Kit-8 (CCK-8). Hela cells were seeded into a 96-well plate at a density of 5000 cells per well. After

seeding the cells, MMS nanoparticles solution (1 mg/ml in MEM medium) was immediately added into a 96-well plate. The final concentrations of MMS nanoparticles were 50, 100 and 200 μg/ml, and the final medium volume in each well was 100 μl. After incubation of cells for 24 h, 10 μl of CCK-8 solution was added into each well, and the cells were incubated for another 3 h. The absorbance at 450 nm was then measured using a microplate reader (Bio-Rad 680, USA). Cytotoxicity was expressed as the percentage of viable cells compared with that of untreated control cells.

2.9 Cell uptake assay

For investigation on cell uptake of MMS nanoparticles, MMS nanoparticles were modified with rhodamine B isothiocynate (RBITC) to form RBITC-MMS nanoparticles. In a typical procedure, $1.0\times10^5$ cells were seeded in a 35-mm petri dish for 4 h to allow the cells to attach. After the cells were washed twice with PBS, RBITC-MMS nanoparticles were added to the petri dishes in a concentration of 100 μg/ml. After incubation for 4 h, the cells were washed several times with PBS to remove the remaining particles and dead cells. Subsequently, the cells were treated for 25 min using 0.5 μg/ml of Hoechst 33342 to stain the nuclei. The cells were washed with PBS to remove extra dye molecules and then fixed with 4% of paraformaldehyde for 20 min. After that, the cells were washed with PBS for 3 times, and observed under a confocal laser scanning microscopy (Leica, Germany).

## 3. Results and discussion

3.1 Characterization of MMS nanoparticles

Fig. 1 shows wide-angle XRD patterns of $Fe_3O_4$ and MMS nanoparticles. $Fe_3O_4$

nanoparticles were initially prepared according to a previously reported method [40], and the crystalline structure can be easily indexed to $Fe_3O_4$ by the XRD pattern. On the patterns of MMS nanoparticles, a broad reflection at $2\theta$=20-25$^o$ suggested the amorphous structure of mesoporous silica matrix, and other well-resolved diffraction peaks were attributed to $Fe_3O_4$ nanoparticles according to the reflection peak positions and relative intensities. The results indicated that the embedded $Fe_3O_4$ nanoparticles retained their crystalline structure after the encapsulation in mesoporous silica matrix.

Fig. 2 shows TEM images of $Fe_3O_4$ and MMS nanoparticles. It can be observed that $Fe_3O_4$ nanoparticles had small particle size ranged from 15 to 20 nm (Fig. 2A), indicating the superparamagnetic behavior, because magnetic $Fe_3O_4$ particles exhibit superparamagnetic behavior when the particle size decreases to below a critical value, generally around 20 nm [46]. MMS nanoparticles were synthesized by using sol-gel technique and hexadecyltrimethylammonium p-toluenesulfonate (CTAT) as structure-directing agent. As shown in Fig. 2B-D, $Fe_3O_4/mSiO_2$-1, $Fe_3O_4/mSiO_2$-2 and $Fe_3O_4/mSiO_2$-3 nanoparticles were spherical and highly monodisperse, the average particle sizes were close to each other, and were estimated to be 150 nm. On the other hand, mesopores could be observed on MMS nanoparticles, and one to several $Fe_3O_4$ nanoparticles were embedded in each MMS nanoparticle. Furthermore, more $Fe_3O_4$ nanoparticles were embedded in mesoporous silica matrix with increasing the addition of $Fe_3O_4$ nanoparticles during the preparation.

Fig. 3 shows $N_2$ adsorption-desorption isotherms of MMS nanoparticles together with the corresponding pore size distributions. These isotherms can be classified as type IV isotherms, demonstrating the mesoporous characteristics of MMS nanoparticles. The BET

surface areas ($S_{BET}$) of the $Fe_3O_4/mSiO_2$-1, $Fe_3O_4/mSiO_2$-2 and $Fe_3O_4/mSiO_2$-3 nanoparticles were 595.6, 508.2 and 464.2 $m^2/g$, respectively. The single point adsorption pore volume ($V_P$) at $P/P_0$=0.97 for the $Fe_3O_4/mSiO_2$-1, $Fe_3O_4/mSiO_2$-2 and $Fe_3O_4/mSiO_2$-3 nanoparticles were 0.859, 0.619 and 0.623 $cm^3/g$, respectively (Table 1). Furthermore, the corresponding pore size distributions of the $Fe_3O_4/mSiO_2$-1, $Fe_3O_4/mSiO_2$-2 and $Fe_3O_4/mSiO_2$-3 nanoparticles exhibited the similar and bimodal pore size distributions, which were consistent with the previous reported mesoporous silica nanoparticles using CTAT as structure directing agent [47-48]. Therefore, the encapsulation of different amount of $Fe_3O_4$ nanoparticles in mesoporous silica matrix did not significantly change mesoporous structure of MMS nanoparticles, which allow anticancer drug molecules to load into the mesoporous channels.

3.2 Magnetic heating capacity of MMS nanoparticles

The magnetic properties of $Fe_3O_4$ and MMS nanoparticles were investigated with a vibrating sample magnetometer (VSM). Fig. 4 shows the magnetization curves measured at 298K. Similar to $Fe_3O_4$ nanoparticles, very small hysteresis loops were observed in the magnetization curves of the $Fe_3O_4/mSiO_2$-1, $Fe_3O_4/mSiO_2$-2 and $Fe_3O_4/mSiO_2$-3 nanoparticles, and the coercivity and the remanence were less than 10 Oe and 0.9 emu/g, respectively, which indicated that the superparamagnetic behavior of $Fe_3O_4$ nanoparticles was maintained throughout the synthesis process. The $Fe_3O_4$ nanoparticles had a magnetization of 43.9 emu/g at 500 Oe. Although the resulting overall saturation magnetization of MMS nanoparticles decreased due to the non-magnetic nature of

mesoporous silica matrix, the $Fe_3O_4/mSiO_2$-1, $Fe_3O_4/mSiO_2$-2 and $Fe_3O_4/mSiO_2$-3 nanoaprticles still showed good magnetic properties, and the saturation magnetization was estimated to be 4.2, 5.8 and 8.1 emu/g, respectively. The results indicated that MMS nanoparticles had potential for generating heat under an alternating magnetic field.

Fig. 5 shows the magnetic heating capacity of $Fe_3O_4$ and MMS nanoparticles evaluated under the magnetic field with frequency of 238 and 409 kHz and magnetic field strength of 150 Gauss with sample concentration of 50 mg/ml in $H_2O$. From the temperature kinetic curves of $Fe_3O_4$ nanoparticles (Fig. 5A-B), the temperature increased from 17 to 80 $^oC$ within 510 and 250 s at the frequency of 238 and 409 kHz, respectively, suggesting that $Fe_3O_4$ nanoparticles can reach the hyperthermia temperature within a very short time under an alternating magnetic field. For MMS nanoparticles, the initial rise in temperature with time was roughly linear then continuously slowed down and the tendency to saturate. The absolute temperature increase in 20 min for MMS nanoparticles at the frequency of 238 and 409 kHz are shown as Fig. 5C. At a frequency of 238 kHz, the absolute temperature increase was estimated to be 6.6, 11.2 and 26 $^oC$ for the $Fe_3O_4/mSiO_2$-1, $Fe_3O_4/mSiO_2$-2 and $Fe_3O_4/mSiO_2$-3 nanoparticles, respectively. At a frequency of 409 kHz, the absolute temperature increase can reach to be 15.5, 29.1 and 43.9 $^oC$ for the $Fe_3O_4/mSiO_2$-1, $Fe_3O_4/mSiO_2$-2 and $Fe_3O_4/mSiO_2$-3 nanoparticles, respectively.

Correspondingly, the magnetic heating capacity of $Fe_3O_4$ and MMS nanoparticles was quantified through the specific absorption rate (SAR). Fig. 5D shows the SAR values of $Fe_3O_4$ and MMS nanoparticles under the magnetic field with frequency of 238 and 409 kHz and magnetic field strength of 150 Gauss. The SAR values of $Fe_3O_4$ nanoparticles at a frequency

of 238 and 409 kHz were estimated to be 16.9 and 27.6 W/g, respectively. Although MMS nanoparticles showed a decreased SAR value compared to $Fe_3O_4$ nanoparticles, the $Fe_3O_4/mSiO_2$-3 nanoparticles still had the SAR values of 4.0 and 9.1 W/g at a frequency of 238 and 409 kHz, respectively. Therefore, the results indicated that MMS nanoparticles also exhibited the magnetic heating capacity, although the magnetic heating capacity of MMS nanoparticles was lower than that of $Fe_3O_4$ nanoparticles. Furthermore, the magnetic heating capacity of MMS nanoparticles followed the sequence of $Fe_3O_4/mSiO_2$-1<$Fe_3O_4/mSiO_2$-2<$Fe_3O_4/mSiO_2$-3 nanoparticles, because the increasing amount of $Fe_3O_4$ nanoparticles was embedded in the $Fe_3O_4/mSiO_2$-1, $Fe_3O_4/mSiO_2$-2 and $Fe_3O_4/mSiO_2$-3 nanoparticles, and thereby increasing the saturation magnetization of MMS nanoparticles. On the other hand, under the fixed magnetic field strength, the magnetic heating capacity of MMS nanoparticles at 409 kHz was much better than at 238 kHz.

Magnetic heating capacities of $Fe_3O_4$ and MMS nanoparticles depending on the magnetic field strength were also investigated in this study. Fig. 6 shows the SAR values of $Fe_3O_4$ and MMS nanoparticles under a magnetic field with a frequency of 409 kHz and magnetic field strength of 90-180 Gauss. It can be observed that the SAR values of $Fe_3O_4$ and MMS nanoparticles increased with an increase of magnetic field strength. For $Fe_3O_4$ nanoparticles, when the magnetic field strength increased from 90 to 180 Gauss, SAR increased from 8.5 to 39.6 W/g. At the same magnetic field strength, MMS nanoparticles exhibited a decrease of SAR value compared to $Fe_3O_4$ nanoparticles due to a large amount of mesoporous silica matrix in MMS nanoparticles, but the SAR values of the $Fe_3O_4/mSiO_2$-3 nanoparticles still increased from 2.9 to 12.1 W/g with increasing the magnetic field

strength from 90 to 180 Gauss. On the other hand, for MMS nanoparticles, the SAR values increased with increasing the $Fe_3O_4$ amount in MMS nanoparticles when applied the same magnetic field strength. Generally, the value of SAR should be as high as possible to minimize the amount of magnetic material applied for hyperthermia. In this study, the $Fe_3O_4/mSiO_2$-3 nanoparticles showed the best magnetic heating capacity among MMS nanoparticles.

3.3 DOX delivery ability of MMS nanoparticles

To investigate the drug delivery ability of MMS nanoparticles, doxorubicin hydrochloride (DOX), an anticancer drug, was used as a model drug to introduce into MMS nanoparticles. The DOX loading amounts in the $Fe_3O_4/mSiO_2$-1, $Fe_3O_4/mSiO_2$-2 and $Fe_3O_4/mSiO_2$-3 nanoparticles were 44.9, 43.9 and 45.4 μg DOX per 1 mg of MMS nanoparticles, respectively. Fig. 7 shows the DOX release from MMS nanoparticles in the release media of pH 7.4 and pH 5.0. It can be observed that DOX release behavior from MMS nanoparticles depended on the pH environment of release medium, and the $Fe_3O_4/mSiO_2$-1, $Fe_3O_4/mSiO_2$-2 and $Fe_3O_4/mSiO_2$-3 nanoparticles showed similar release behavior.

In the release medium of pH 7.4, the DOX releases from MMS nanoparticles were very slow and only ca. 7-8% of DOX were released after 23 h. While in the release medium of pH 5.0, the DOX release rate exhibited an increase, and ca. 55-65% of DOX were released after 23 h. It might be that DOX molecules were adsorbed on the mesopore surface of MMS nanoparticles via the electrostatic interaction and hydrogen bonding. When lowering of pH

value in release medium, the interaction forces between DOX and silica could decrease due to the protonation of surface silanols, which result in the easier detachment of DOX molecules in the acidic environment, and thereby increase the DOX release rate.

Generally, the pH environment out of cancer cells is near pH 7.4, while the endosome/lysosome and cytosol in cells is estimated to be pH 5.0-5.5. Therefore, such drug release behavior is very important for an efficient and nontoxic drug delivery system, because the slow release at pH 7.4 might decrease the DOX release during the transport of the drug delivery system in blood stream, while much faster DOX release at acid pH on arriving at the targeted cancer cells. Therefore, MMS nanoparticles as carries for DOX delivery would be beneficial for chemotherapy.

3.4 In vitro cytotoxicity and cell uptake

The cytotoxicity evaluation of drug delivery vehicles is critical for drug delivery. In this study, in vitro cytotoxicity of MMS nanoparticles to Hela cells was evaluated using Cell Counting Kit-8 (CCK-8) assay. As shown in Fig. 8, cell viabilities after 24 h of incubation were similar for the $Fe_3O_4/mSiO_2$-1, $Fe_3O_4/mSiO_2$-2 and $Fe_3O_4/mSiO_2$-3 nanoaprticles. It can also be observed that cell viabilities exhibited a slight decrease with the increasing the concentrations of MMS nanoparticles, but they did not have a significant difference even up to a concentration of 200 μg/ml compared to the control group, which indicated that MMS nanoparticles had low cytotoxicity and could be used as carriers for DOX delivery. It might be that the protection of $Fe_3O_4$ nanoparticles by mesoporous silica matrix contributes the low cytotoxicity of MMS nanoparticles. He et al. reported that mesoporous silica

nanoparticles exhibited low cytotoxicity even at a concentration of 500 μg/ml and would be safe for drug delivery [49].

It is very important for MMS nanoparticles to be taken up by cancer cells. One hand, cell uptake of MMS nanoparticles could facilitate local magnetic hyperthermia owning to magnetic heating in cancer cells. On the other hand, cell uptake of MMS nanoparticles could also be beneficial for chemotherapy due to the enhancement of the intracellular delivery of DOX, and thereby enhancing the anticancer activity of DOX. In this study, to verify the cell uptake of MMS nanoparticles, MMS nanoparticles were modified with rhodamine B isothiocynate (RBITC) to form RBITC-MMS nanoparticles, and RBITC-MMS nanoparticles were incubated with Hela cells for 4 h. As shown in Fig. 9, red fluorescence from RBITC-MMS nanoparticles were distributed in the cells and primarily located between cell membrane and nucleus, which suggest that RBITC-MMS nanoparticles were taken up into Hela cells after endocytosis. Furthermore, no significant difference could be observed among the $Fe_3O_4/mSiO_2$-1, $Fe_3O_4/mSiO_2$-2 and $Fe_3O_4/mSiO_2$-3 nanoparticles due to their similar particle size and surface chemistry. Therefore, loading of anticancer drugs in MMS nanoparticles to deliver in cancer cells could significantly enhance the efficiency of drug delivery and magnetic hyperthermia, and thereby promote cancer therapy.

## 4. Conclusion

In this study, we have developed a MMS nanoparticle-based drug delivery system for potential chemotherapy and hyperthermia. MMS nanoparticles had the average particle size of 150 nm, and showed low cytotoxicity and efficient cell uptake ability. Using DOX as a

model drug, the DOX-loaded MMS nanoparticles were capable of drug release in the medium of pH 5.0, mimicking the environment in cancer cells, but very slow release in the medium of pH 7.4. On the other hand, MMS nanoparticles could efficiently generate heat upon exposure to an alternating magnetic field due to the superparamagnetic behavior. Furthermore, magnetic heating capacity of MMS nanoparticles could be turned due to the controllable magnetization of MMS nanoparticles, and the SAR of the $Fe_3O_4$/m$SiO_2$-3 nanoparticles was estimated to be 12.1 W/g under an alternating magnetic field with frequency of 409 kHz and magnetic field strength of 180 Gauss with sample concentration of 50 mg/ml in $H_2O$. Therefore, MMS nanoparticles could provide a promising platform for the combination of chemotherapy and hyperthermia for cancer therapy.

**Acknowledgements**

The authors gratefully acknowledge the support by the Program for Professor of Special Appointment (Eastern Scholar) at Shanghai Institutions of Higher Learning, National Natural Science Foundation of China (No. 51102166), Shanghai Shuguang Project (No. 12SG39), Program for New Century Excellent Talent in University (No. NCET-12-1053), Key Project of Chinese Ministry of Education (No. 212055), Innovation Program of Shanghai Municipal Education Commission (No. 12ZZ140), the Hujiang Foundation of China (No. B14006) and Training Program of University of Shanghai for Science and Technology (No. 14XPY01).

**References:**

[1] D. Jelovac, D. K. Armstrong, *CA Cancer J. Clin*. 2011, **61**, 183-203.

[2] M. H. Falk, R. D. Issels, *Int. J. Hyperthermia*, 2001, **17**, 1-18.

[3] T. Kobayashi, *Biothechnol. J.* 2011, **6**, 1342-1347.

[4] P. Drake, H.-J. Cho, P.-S. Shih, C.-H. Kao, K.-F. Lee, C.-H. Kuo, X.-Z. Lin, Y. J. Lin, *J. Mater. Chem*. 2007, **17**, 4914-4918.

[5] M. Zhang, O, B. Garbuzenko, K. R. Reuhl, L. Rodriguez-Rodriguez, T. Minko, *Nanomedicine*, 2012, **7**, 185-197.

[6] N. H. Levi-Polyachenko, J. H. Stewart, *Open Nanomed. J*. 2011, **3**, 24-37.

[7] H. Lee, S. Kim, B.-H. Choi, M.-T. Park, J. Lee, S.-Y. Jeong, E. K. Choi, B.-U. Lim, C. Kim, H. J. Park, *Int. J. Hyperthermia*, 2011, **27**, 698-707.

[8] O. Taratula, R. K. Dani, C. Schumann, H. Xu, A. Wang, H. Song, P. Dhagat, O. Taratula, *Int. J. Pharm*. 2013, **458**, 169-180.

[9] Y. Ren, H. Zhang, B. Chen, J. Cheng, X. Cai, R. Liu, G. Xia, W. Wu, S. Wang, J. Ding, C. Gao, J. Wang, W. Bao, L. Wang, L. Tian, H. Song, X. Wang, *Int. J. Nanomed*. 2012, **7**, 2261-2269.

[10] P. Kulshrestha, M. Gogoi, D. Bahadur, R. Banerjee, *Colloids Surf. B*, 2012, **96**, 1-7.

[11] P. Pradhan, J. Giri, F. Rieken, C. Koch, O. Mykhaylyk, M. Doblinger, R. Banerjee, D. Bahadur, C. Plank, *J. Controlled Release* 2010, **142**, 108-121.

[12] C. S. S. R. Kumar, F. Mohammad, *Adv. Drug Del. Rev*. 2011, **63**, 789-808.

[13] M. Bonini, D. Berti, P. Baglioni, *Current Opinion Colloid Interface Sci*. 2013, **18**, 459-467.

[14] K. Hayashi, K. Ono, H. Suzuki, M. Sawada, M. Moriya, W. Sakamoto, T. Yogo, *ACS Appl. Mater. Interfaces*, 2010, **2**, 1903-1911.

[15] A. M. Derfus, G. Von Maltzahn, T. J. Harris, T. Duza, K. S. Vecchio, E. Ruoslahti, S. N. Bhatia, *Adv. Mater*. 2007, **19**, 3932-3936.

[16] C. S. Brazel, *Pharm. Res*. 2009, **26**, 644-656.

[17] S. Purushotham, R. V. Ramanujan, *Acta Biomater*. 2010, **6**, 502-510.

[18] S. R. Deka, A. Quarta R. Di Corato, A. Riedinger, R. Cingolani, T. Pellegrino, *Nanoscale,* 2011, **3**, 619-629.

[19] M. P. Leal, A. Torti, A. Riedinger, R. L. Fleur, D. Petti, R. Cingolani, R. Bertacco, T. Pellegrino, *ACS Nano*, 2012, **6**, 10535-10545.

[20] C. E. Nelson, J. R. Kintzing, A. Hanna, J. M. Shannon, M. K. Gupta, C. L. Duvall, *ACS Nano*, 2013, **7**, 8870-8880.

[21] A. Villanueva, P. de la Presa, J. M. Alonso, T. Rueda, A. Martinez, P. Crespo, M. P. Morales, M. A. Gonzalez-Fernandez, J. Valdes, G. Rivero, *J. Phys. Chem. C*, 2010, **114**, 1976-1981.

[22] S.-H. Hu, T.-Y. Liu, H.-Y. Huang, D.-M. Liu, S.-Y. Chen, *Langmuir*, 2008, **24**, 239-244.

[23] L. H. Reddy, J. L. Arias, J. Nicolas, P. Couvreur, *Chem. Rev*. 2012, **112**, 5818-5878.

[24] S. Murakami, T. Hosono, B. Jeyadevan, M. Kamitakahara, K. Ioku, *J. Ceram. Soc. Japan*, 2008, **116**, 950-954.

[25] K. Ariga, A. Vinu, Y. Yamauchi, Q. Ji, J. P. Hill, *Bul. Chem. Soc. Japan*, 2012, **85**, 1-32.

[26] D. Tarn, C. E. Ashley, M. He, E. C. Cames, J. I. Zink, C. J. Brinker, *Accounts Chem. Res*. 2013, **46**, 792-801.

[27] B.-S. Lee, L.-C. Huang, C.-Y. Hong, S.-G. Wang, W.-H. Hsu, Y. Yamauchi, C.-J. Hsieh, J.-Y. Lai, K. C.-W. Wu, *Acta Biomater*. 2011, **7**, 2276-2284.

[28] P. Yang, S. Gai, J. Lin, *Chem. Soc. Rev*. 2012, **41**, 3679-3698.

[29] C. Hom, J. Lu, F. Tamanoi, *J. Mater. Chem*. 2009, **19**, 6308-6318.

[30] A. K. Gupta, M. Gupta, *Biomaterials*, 2005, **26**, 3995-4021.

[31] W. Zhao, J. Gu, L. Zhang, H. Chen, J. Shi, *J. Am. Chem. Soc*. 2005, **127**, 8916-8917.

[32] H. Wu, S. Zhang, J. Zhang, G. Liu, J. Shi, L. Zhang, X. Cui, M. Ruan, Q. He, W. Bu, *Adv. Funct. Mater.* 2011, **21**, 1850-1862.

[33] J. Liu, S. Z. Qiao, S. B. Hartono, G. Q. Lu, *Angew. Chem. Int. Ed*. 2010, **49**, 4981-4985.

[34] B. Julian-Lopez, C. Boissiere, C. Chaneac, D. Groso, S. Vasseur, S. Miraux, E. Duguet, C. Sanchez, *J. Mater. Chem*. 2007, **17**, 1563-1569.

[35] K. C. Souza, N. D. S. Mohallem, E. M. B. Sousa, J. Sol-Gel Sci. Technol. 2010, 53, 418-427.

[36] E. Ruiz-Hernandez, A. Lopez-Noriega, D. Arcos, I. Izquierdo-Barba, O. Terasaki, M. Vallet-Regi, *Chem. Mater*. 2007, **19**, 3455-3463.

[37] F. M. Martin-Saavedra, E. Ruiz-Hernandez, A. Bore, D. Arcos, M. Vallet-Regi, N. Vilaboa, *Acta Biomater.* 2010, **6**, 4522-4531.

[38] F. Lu, A. Popa, S. Zhou, J.-J. Zhu, A. C. S. Samia, Chem. Commun. 2013, 49, 11436-11438.

[39] A. S. Al-Kady, M. Gaber, M. M. Hussein, E.Z. M. Ebeid, *Euro. J. Pharm. Biopharm*. 2011, **77**, 66-74.

[40] A. Baeza, E. Guisasola, E. Ruiz-Hernandez, M. Vallet-Regi, *Chem. Mater*. 2012, **24**, 517-524.

[41] J. Liu, C. Detrembleur, M.-C. De Pauw-Gillet, S. Mornet, L. V. Elst, S. Laurent, C. Jerome, E. Duguet, *J. Mater. Chem. B*, 2014, **2**, 59-70.

[42] J. Zhang, W. Sun, L. Bergman, J. M. Rosenholm, M. Linden, G. Wu, H. Xu, H.-C. Gu, *Matter. Lett*. 2012, **67**, 379-382.

[43] [2] Y.C. Lee, C.-T. Chen, Y.-T. Chiu, K. C.-W. Wu, *ChemCatChem*, 2013, **5**, 2153-2157.

[44] H. Jiang, P. Chen, S. Luo, X. Tu, Q. Cao, Y. Zhou, W. Zhang, *J. Inorg. Org. Polym. Mater.* 2013, **23**, 393-400.

[45] M. R. Lohe, K. Gedrich, T. Freudenberg, E. Kockrick, T. Dellmann, S. Kaskel, *Chem. Commun*. 2011, **47**, 3075-3077.

[46] Y. P. He, S. Q. Wang, C. R. Li, Y. M. Miao, Z. Y. Wu, B. S. Zou, *J. Phys. D: Appl. Phys.* 2005, **38**, 1342.

[47] K. Zhang, L.-L. Xu, J.-G. Jiang, N. Calin, K.-F. Lam, S.-J. Zhang, H.-H. Wu, G.-D. Wu, B. Albela, L. Bonneviot, P. W, *J. Am. Chem. Soc*. 2013, **135**, 2427-2430.

[48] C. Tao, Y. Zhu, Y. Xu, M. Zhu, H. Morita, N. Hanagata, *Dalton Trans*. 2014, **43**, 5142-5150.

[49] Q. He, Z. Zhang, Y. Gao, J. Shi, Y. Li, *Small*, 2009, **5**, 2722-2729.

Table 1 Structural parameters and DOX loading of MMS nanoparticles

| Samples | $S_{BET}$ ($m^2$/g) | $V_P$ ($cm^3$/g) | $D_p$ (nm) | DOX loading (μg/mg) |
|---|---|---|---|---|
| $Fe_3O_4$/m$SiO_2$-1 | 595.6 | 0.859 | 3.2/12.5 | 44.9 |
| $Fe_3O_4$/m$SiO_2$-2 | 508.2 | 0.619 | 3.4/7.9 | 43.9 |
| $Fe_3O_4$/m$SiO_2$-3 | 464.2 | 0.623 | 3.4/10.7 | 45.4 |

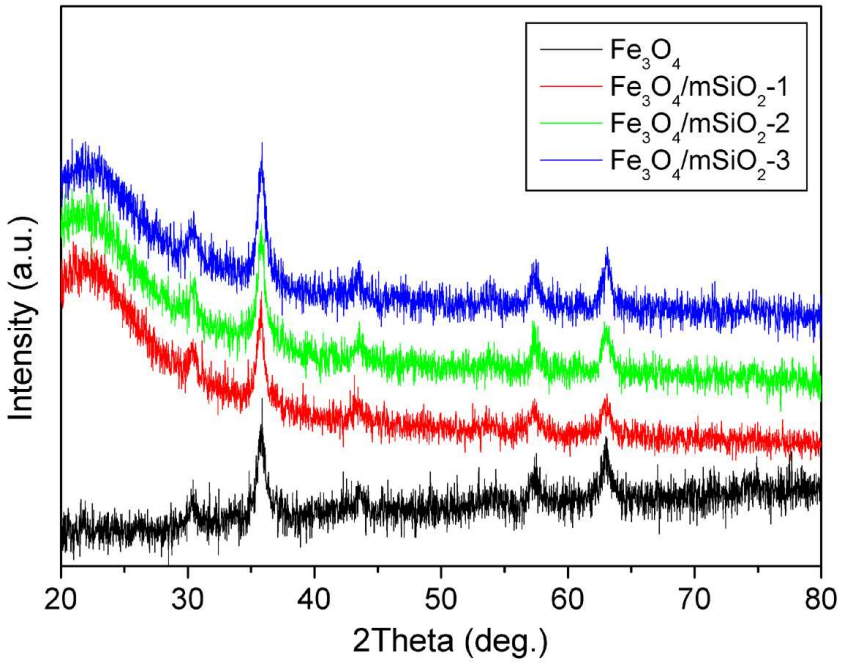


Fig. 1 Wide-angle XRD patterns of $Fe_3O_4$ and MMS nanoparticles.

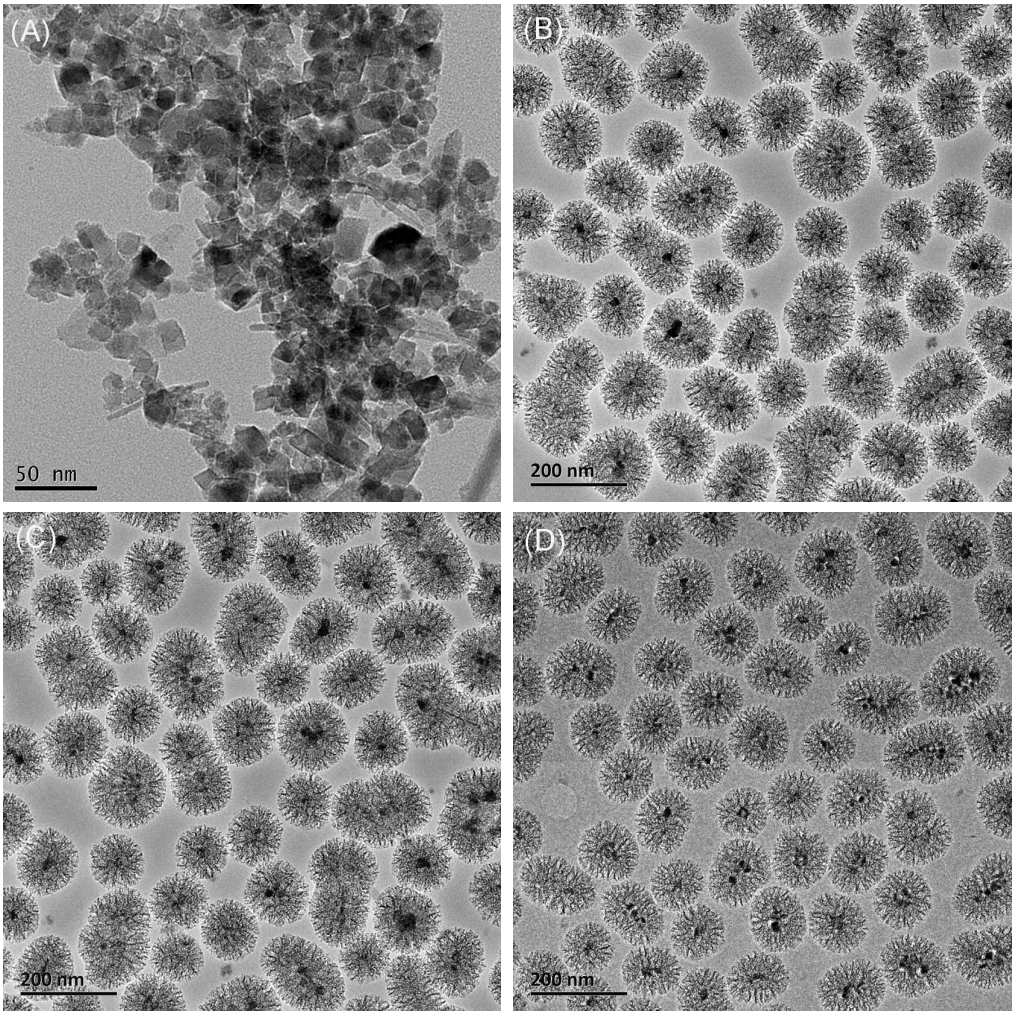


Fig. 2 TEM images of $Fe_3O_4$ and MMS nanoparticles: (A) $Fe_3O_4$; (B) $Fe_3O_4/mSiO_2$-1; (C) $Fe_3O_4/mSiO_2$-2 and (D) $Fe_3O_4/mSiO_2$-3 nanoaprticles.

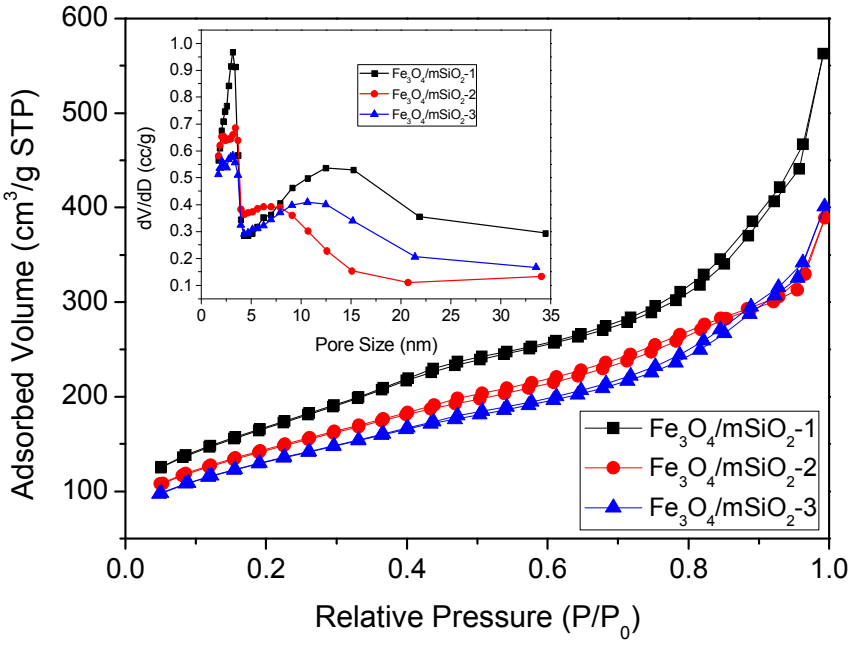


Fig. 3 $N_2$ adsorption-desorption isotherms of MMS nanoparticles and corresponding pore size distributions (insert).

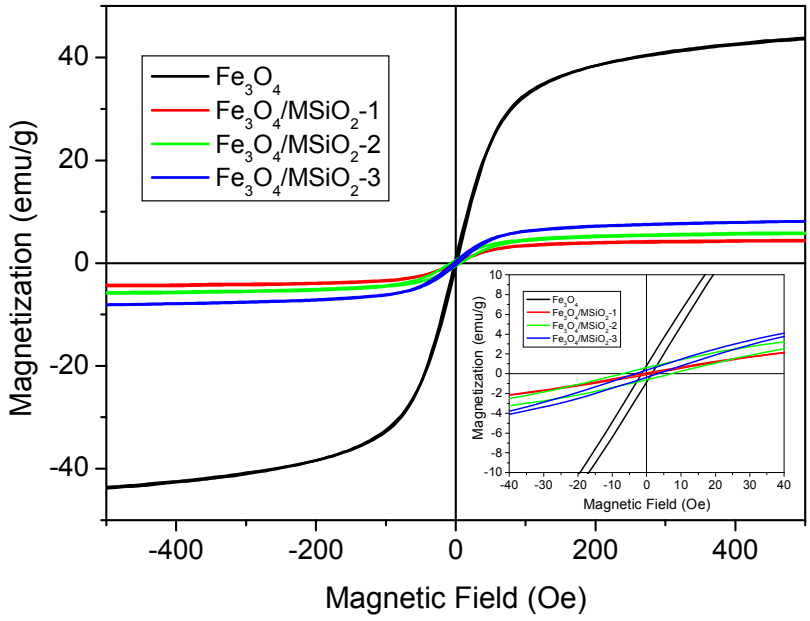


Fig. 4 Magnetization curves of $Fe_3O_4$ and MMS nanoparticles measured at 298K.

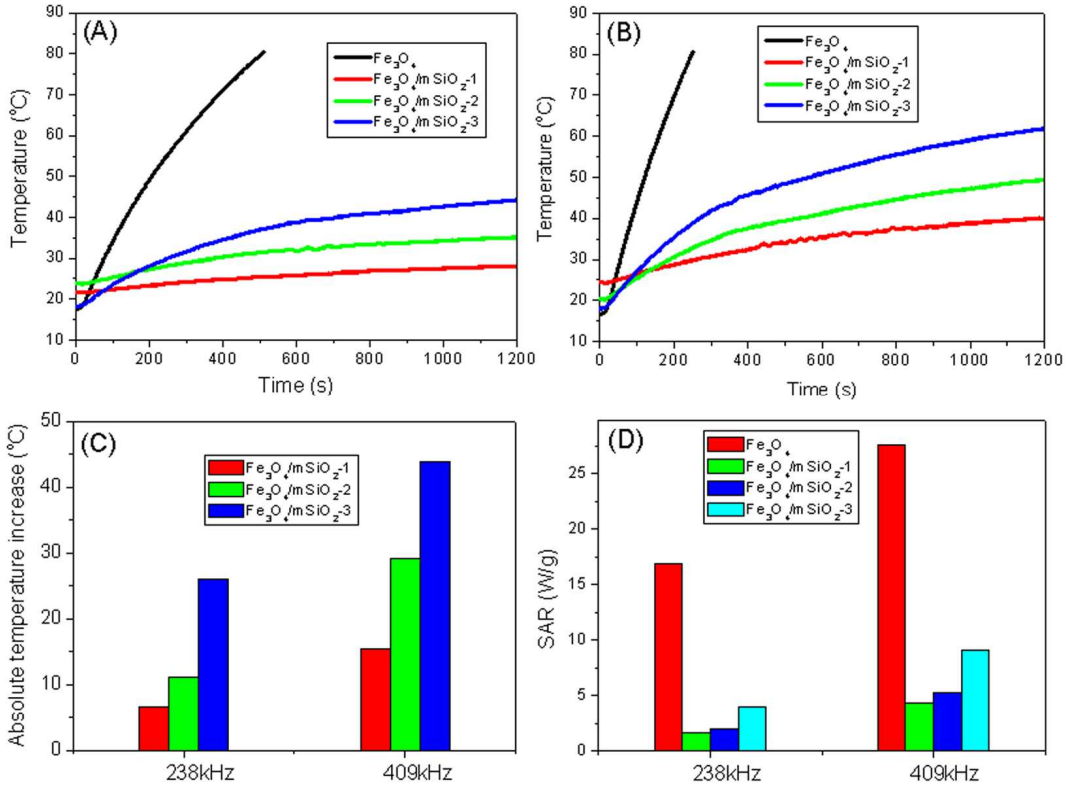


Fig. 5 the magnetic heating capacity of $Fe_3O_4$ and MMS nanoparticles evaluated under the alternating magnetic field with sample concentration of 50 mg/ml: (A) and (B) temperature vs. time curves for $Fe_3O_4$ and MMS nanoparticles at frequency of 238 kHz and 409 kHz under fixed applied field of 150 Gauss; (C) the absolute temperature increases of MMS nanoparticles at frequency of 238 kHz and 409 kHz under fixed applied field of 150 Gauss for 20 min; (D) the SAR values of $Fe_3O_4$ and MMS nanoparticles at frequency of 238 kHz and 409 kHz under fixed applied field of 150 Gauss.

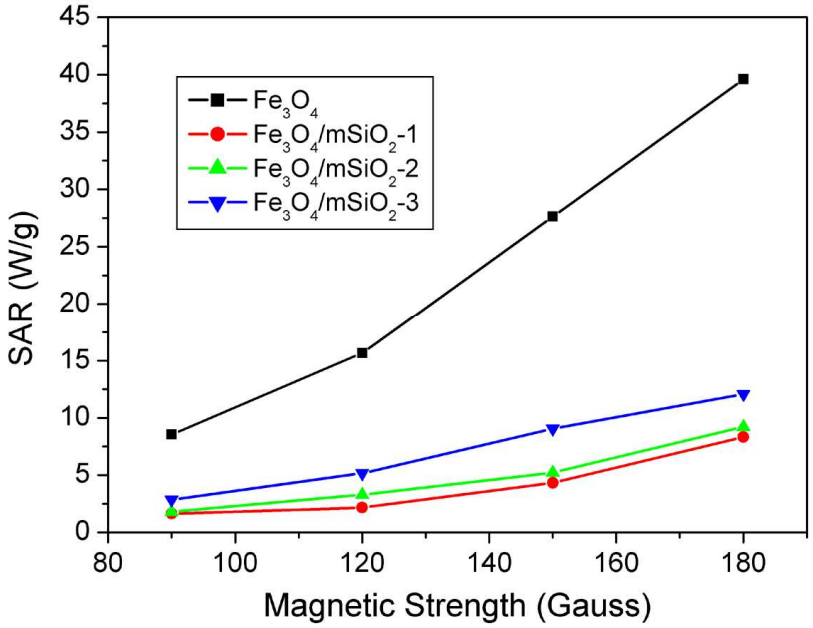


Fig. 6 SAR values of $Fe_3O_4$ and MMS nanoparticles evaluated under the alternating magnetic field at fixed frequency of 409 kHz under the applied field of 90-180 Gauss with sample concentration of 50 mg/ml in $H_2O$.

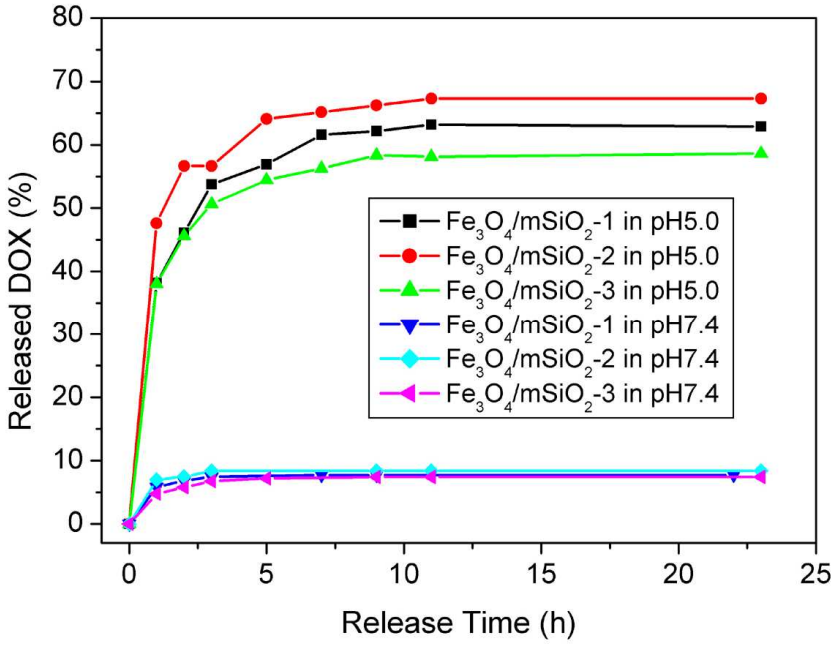


Fig. 7 DOX release from MMS nanoparticles in the release media of pH 7.4 and pH 5.0, respectively.

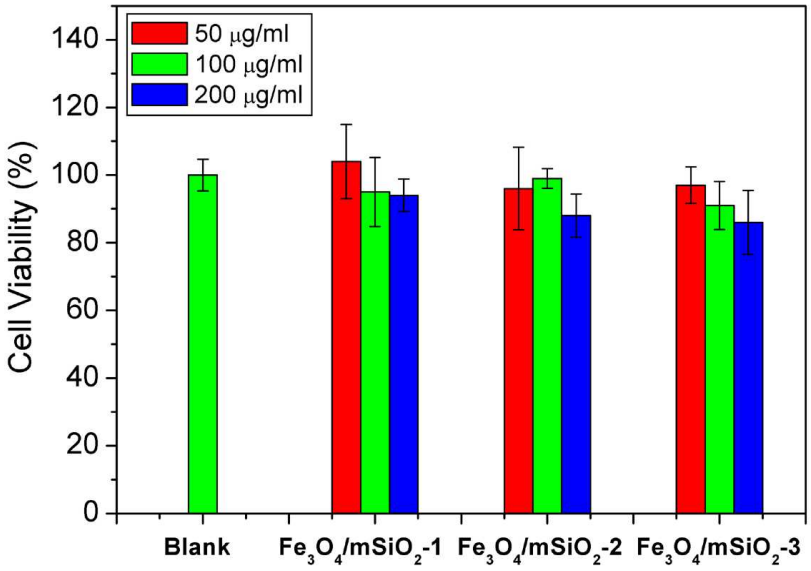


Fig. 8 Effect of the concentrations of MMS nanoparticles on the cytotoxicity to Hela cells, as measured by a Cell Counting Kit-8 assay.

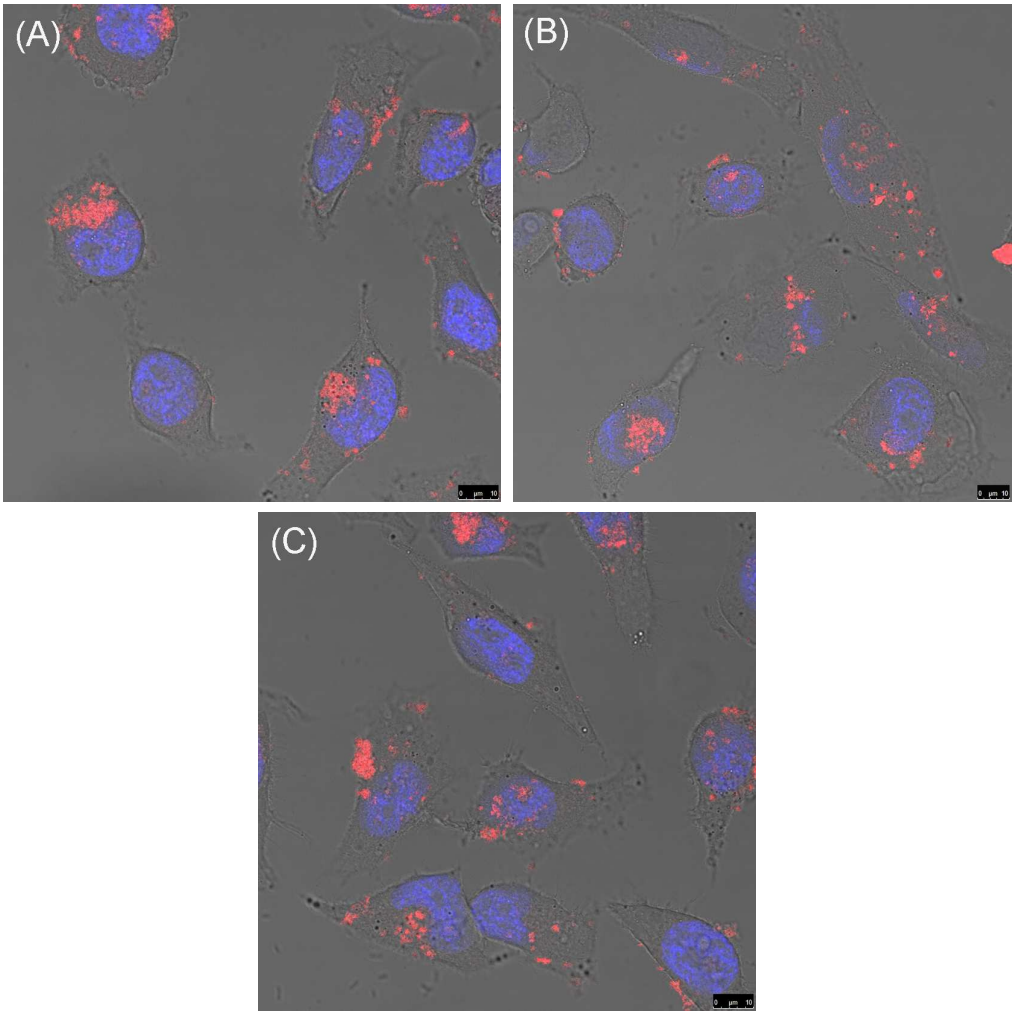


Fig. 9 Confocal microscope images of Hela cells after 4 h of incubation with MMS nanoparticles: (A) $Fe_3O_4/mSiO_2$-1, (B) $Fe_3O_4/mSiO_2$-2 and (c) $Fe_3O_4/mSiO_2$-3 nanoparticles.

A Table of Contents Entry

Title: Magnetic Mesoporous Silica Nanoparticles for Potential Delivery of Chemotherapeutic Drugs and Hyperthermia

Authors: Cuilian Tao, Yufang Zhu

TOC Figure:

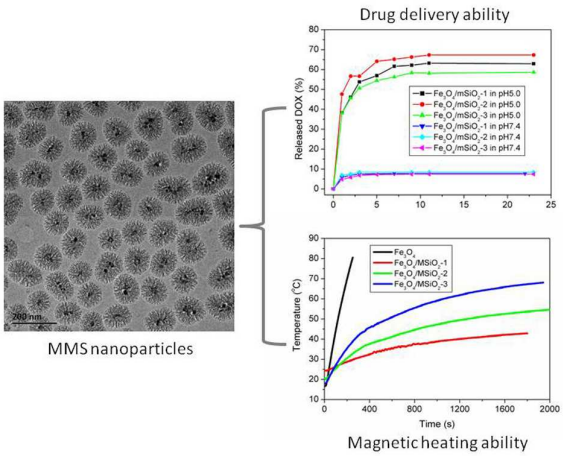


Text: Magnetic mesoporous silica (MMS) nanoparticles could provide a promising multifunctional platform for the combination of chemotherapy and hyperthermia.